

# **A ductile fracture model considering stress state and Zener-Hollomon parameter for hot forming of metallic materials**

Xiaoqing Shang <sup>a, b</sup>, Zhenshan Cui <sup>b, \*</sup>, M.W. Fu <sup>a, c, \*\*</sup>

<sup>a</sup> Department of Mechanical Engineering, The Hong Kong Polytechnic University, Hung Hom, Kowloon, Hong Kong

<sup>b</sup> National Engineering Research Center of Die and Mold CAD, Shanghai Jiao Tong University, 1954 Huashan Road, Shanghai 200030, P.R. China

<sup>c</sup> PolyU Shenzhen Research Institute, No. 18 Yuexing Road, Nanshan District, Shenzhen, P.R. China

## **Abstract**

To articulate the ductile fracture behavior and predict its occurrence in hot deformation of metallic materials, the initiation condition of ductile fracture in hot working was identified by experiments, and an extended fracture model for analysis of deformation and fracture in hot forming of metallic materials was established and validated. Firstly, experiments were conducted for 316LN stainless steel at elevated temperatures and the dynamic recrystallization (DRX) affected ductility was determined for the material. Via using the Zener–Hollomon ( $Z$ ) parameter to represent the temperature and strain rate dependent DRX behavior, the relationship between ductility and  $Z$  parameter in different DRX conditions was examined and identified. In the deformation of the material with DRX, the ductility of the material decreases with the increase of  $Z$  parameter. In the deformation without DRX, however, the ductile fracture behavior is independent of  $Z$  parameter. An extended fracture model for hot working of metallic materials was thus established by incorporating the  $Z$  parameter and the influence of DRX into a stress based fracture model. For the DRX involved deformation, fracture strain was then designated as a function of stress state,  $Z$  parameter and the percentage of DRX. As for the deformation without DRX, the ductility of materials was considered to be only affected by stress state. The model was then embedded

into finite element (FE) simulation and corroborated via tailor-designed validation experiments. To validate and verify the developed model, a case study of hot forging of a pressure vessel head was employed. The tendency of fracture initiation in the hot forging process was analyzed using the developed model and the design of hot working process was thus optimized with the help of the developed model.

**Keywords:** Extended ductile fracture model; Hot metal forming; Zener-Hollomon parameter; Stress state.

Corresponding authors:

\* Zhenshan Cui;

Tel.: +86-021-62827605, E-mail: [cuizs@sjtu.edu.cn](mailto:cuizs@sjtu.edu.cn)

\*\* M.W. Fu;

Tel.: +852-27665527, E-mail: [mmmwfu@polyu.edu.hk](mailto:mmmwfu@polyu.edu.hk)

## 1. Introduction

Hot forming of metal materials has been widely used for producing complex parts, accompanied with an excellent formability of the materials in the process. However, the non-uniform distribution of temperature, strain and strain rate in the working process often brings about the inhomogeneous deformation and results in the occurrence of ductile fracture. Ductile fracture greatly deteriorates the formability of materials and has thus become a non-trivial issue in deformation-based manufacturing arena. To describe the ductile fracture behavior and predict the fracture occurrence, ductile fracture criteria (DFC) were established and used in different deformation scenarios. In cold working, the ductility of materials is greatly affected by stress state. In hot working process, working temperature and strain rate play an important role affecting the deformation and fracture behavior of metallic materials [1]. Figuring out the relationship between ductility and working conditions and establishing a feasible DFC for hot working of metallic materials is of great importance for providing an in-depth understanding of ductile fracture and optimizing the design of hot forming process for production of defect-free products.

Recently, extensive studies have been conducted to investigate ductile fracture in cold deformation and a number of stress state dependent DFCs were developed. In earlier studies, the maximum principal stress and the mean stress were considered as key influential factors on ductile fracture and employed in development of ductile fracture models, such as Cockcroft and Latham model [2], Oyane model [3], Ayada model [4] and Brozzo model [5]. Afterwards, the non-negligible effect of deviatoric stress on ductile fracture was figured out [6, 7] and taken into consideration in the fracture model development done by Xue [8], Bai and Wierzbicki [9], and Lou et al. [10, 11]. From the micro-mechanism viewpoint, the formation of ductile fracture is a process of void evolution and the void-based ductile fracture

model was thus established with the efforts of [Gurson, Tvergaard and Needleman \[12-14\]](#). The void-based Gurson-Tvergaard-Needleman (GTN) plasticity theory shed light on articulating macroscopic ductile fracture phenomenon with microscopic void evolution and has attracted a lot of efforts to extend its application [\[15-18\]](#). Regarding the reliability of the proposed DFCs, systematic studies were carried out to identify the efficiency and application condition of the developed DFCs [\[19, 20\]](#). Further examination for the applicability of the developed DFCs was conducted in practical forming practices, such as spinning of titanium tube [\[21\]](#), sheet metal forming [\[22\]](#) and incremental forming of aluminum alloys [\[23\]](#).

Ductile fracture models for hot deformation of metallic materials are usually established on the basis of cold deformation fracture models via considering the influence of temperature and strain rate. The pioneering work for modeling and predicting the ductile fracture at elevated temperature was carried out by [Johnson and Cook \[24\]](#). In their work, temperature and strain rate were normalized and introduced into the expression of fracture strain. [Valoppi et al. \[25\]](#) extended the Johnson and Cook model for fracture prediction in hot deformation of titanium alloys by considering the influence of deviatoric stress and phase transformation. In addition, [He et al. \[26\]](#) developed a new hot forming DFC via proposing a temperature and strain rate affected critical damage factor and incorporated the damage factor into the Oyane criterion. The Oyane criterion was also modified by [Novella et al. \[27\]](#) for analyzing the fracture behavior of aluminum alloys in cross wedge rolling process at high temperature. In the work of [Zhu et al. \[28\]](#),  $Z$  parameter was adopted to represent the combined effect of temperature and strain rate and introduced into Oh's fracture model [\[29\]](#). Furthermore, [Alexandrov et al. \[30\]](#) examined the dependency of ductile fracture on  $Z$  parameter and developed a new fracture criterion for hot forming of metallic materials. For the micro-mechanism related ductile fracture, [Sun et al. \[31\]](#) discussed the influence of dynamic

recovery and strain hardening on fracture behavior and established a damage-viscoplasticity constitutive model. With the efforts of the authors [32], the effect of DRX on ductility of materials was explained and a new DFC considering the DRX affected void evolution was established based on the GTN-Thomason model.

Due to the increasing demand for reliable hot deformed and high quality products, an efficient ductile fracture model with a wide applicability is of an urgent need. However, extensive studies have not yet been conducted on modeling of the ductile fracture in hot working process and the understanding of fracture initiation in different deformation scenarios is still superficial. This study is thus focused on the investigating of the relationship between ductile fracture and working conditions and establishing a feasible fracture prediction model for hot forming of metallic materials. The stainless steel 316LN was therefore used as the testing material and its ductility at high temperature was identified by experiments. By employing  $Z$  parameter to represent the comprehensive effect of temperature and strain rate, the dependency of ductility on  $Z$  parameter in various DRX conditions was figured out. An extended DFC for hot deformation was then established via introducing  $Z$  parameter and the percentage of DRX ( $X_{drx}$ ) into a stress based fracture model proposed by Lou et al. [10, 11]. The extended model was then embedded into FE simulation, and the validation and verification of the model were done by the validation experiments and the application of the model in a real industrial case study.

## **2. Experimental methodology**

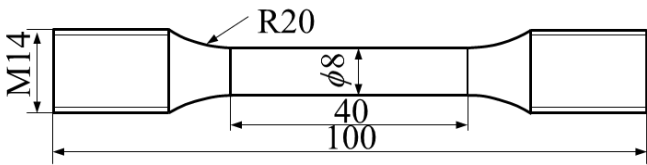
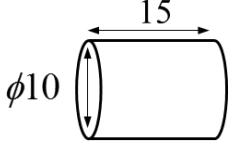
### **2.1 Experimental procedure**

In this study, the as-forged 316LN stainless steel with the mono-austenite microstructure was utilized for testing. To investigate the mechanical properties of the material at elevated

temperatures, tensile and compression experiments were conducted in general hot working parameter window and the detailed design of the experiments is shown in Table 1. Hot tensile experiments were carried out at different temperatures and strain rates to identify the ductility of the material, and the testing sample for hot tension is the dog-bone specimen with a gauge length of 15 mm. The relationship between ductility and working conditions was examined in terms of Z parameter and the value of Z parameter was determined via hot compression tests. High temperature experiments were conducted on Gleeble 1500D thermo-mechanical simulator and water quench was performed on specimens immediately after the tests to retain microstructure.

**Table 1**

Design of experiments conducted at high temperature.

Hot tensile tests	Hot compression tests
Objective: Examining ductility in hot deformation	Determining Z parameter
	
Test condition: 1073 K - 1473 K; 0.01 s <sup>-1</sup> - 3.5 s <sup>-1</sup>	1223 K - 1523 K; 0.001 s <sup>-1</sup> - 1 s <sup>-1</sup>

## 2.2 Determination of flow stress and fracture strain via hot tensile tests

To characterize the ductility of the material in hot tensile tests, the fracture strain, i.e., the maximum equivalent plastic strain at the fracture point, was adopted as the representative parameter. To obtain the fracture strain, simulation was conducted for hot tensile experiments and the flow stress curves used for simulation were calibrated by correlating the simulation outputs to measured ones in aspects of load-stroke curves and the profiles of necking zones.

Fig. 1 presents the determined flow curves for the tested 316LN at elevated temperatures.

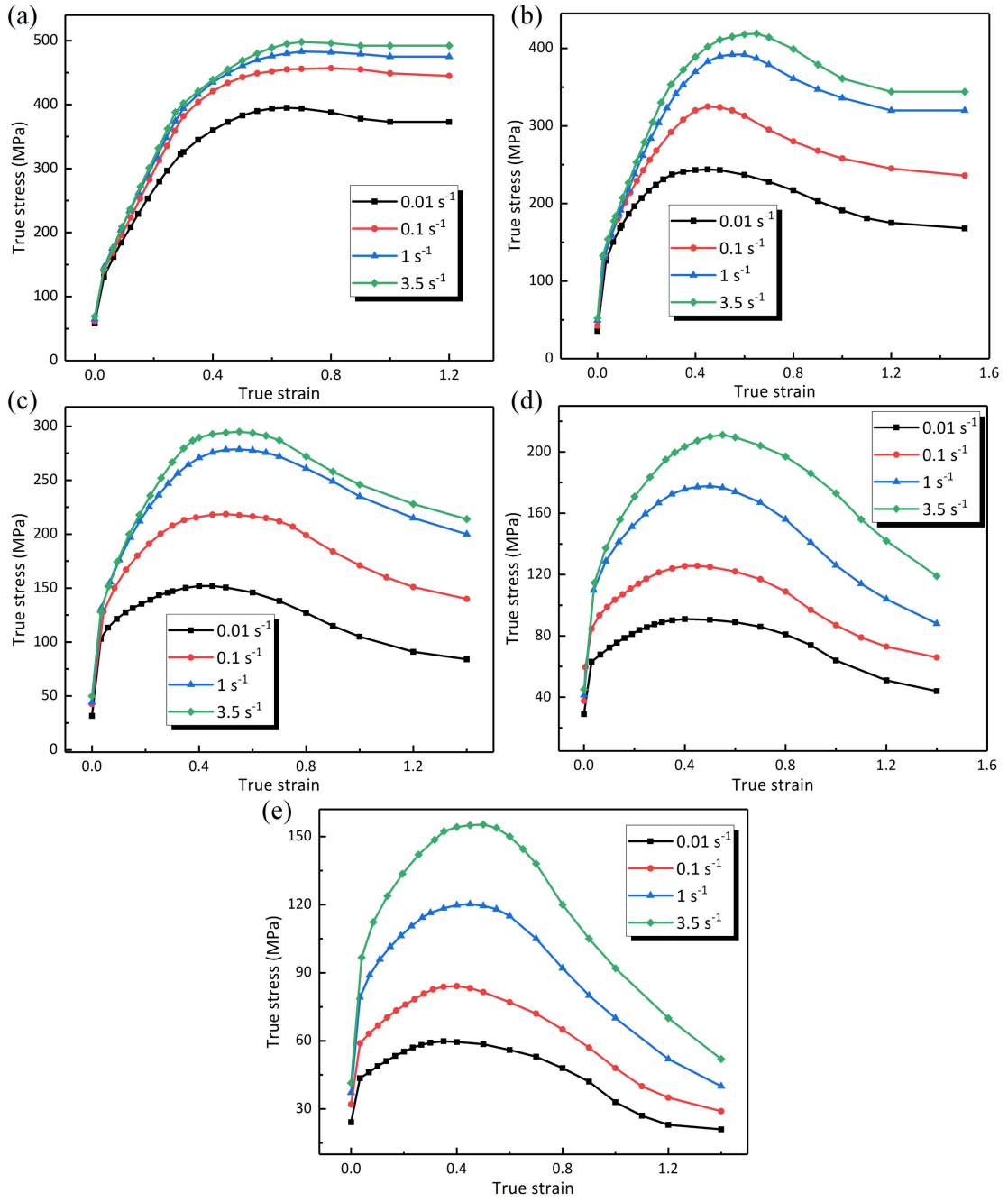


**Fig. 1.** Flow stress curves in hot deformation of 316LN: (a) 1073 K, (b) 1173 K, (c) 1273 K, (d) 1373 K, and (e) 1473 K.

With the determined flow curves, a good consistency of load-stroke curves and the specimen profile at the fracture point between experimental and simulated consequences was obtained for the tests. Fig. 2 exhibits the comparison results and the determined fracture conditions for experiments conducted at conditions of 1273 K - 1 s<sup>-1</sup> and 1373 K - 0.01 s<sup>-1</sup> as examples for

hot tensile tests. In simulation, the fracture point is defined as the moment when the simulated gauge displacement reaches experimental fracture stroke and the fracture strain is the maximum equivalent strain at the fracture point. The simulated fracture strain for all the hot tensile experiments is listed in Table 2 and it is evident that fracture strains of the material change with temperature and strain rate. Further examination for the dependency of fracture strain on hot working parameters was conducted via considering Z parameter and DRX.

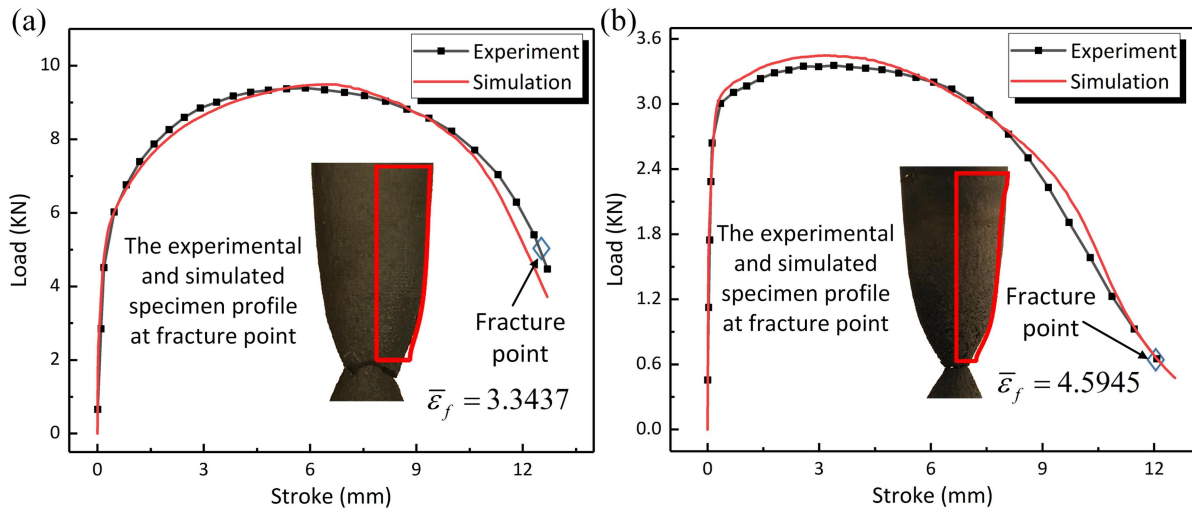


**Fig. 2.** Comparison of load-stroke curves and specimen profile at the fracture point between experimental and simulated consequences for experiments conducted at the condition of: (a) 1273 K - 1 s<sup>-1</sup>, and (b) 1373 K - 0.01 s<sup>-1</sup>.

**Table 2**

Fracture strain for hot tensile experiments.

Strain rate Temperature	0.01 s <sup>-1</sup>	0.1 s <sup>-1</sup>	1 s <sup>-1</sup>	3.5 s <sup>-1</sup>
1073 K	2.3290	2.2146	1.8766	1.9545
1173 K	2.9192	2.7785	2.3109	2.1331
1273 K	3.8045	3.5367	3.3437	2.9737
1373 K	4.5945	4.4651	4.1677	3.5185
1473 K	5.0848	5.3481	4.1609	4.0656



### 2.3 Determination of $Z$ parameter via hot compression tests

$Z$  parameter is also known as the temperature compensated strain rate, which has been widely used for characterizing behaviors of materials in hot working. In studies of [Zhu et al. \[28\]](#) and [Alexandrov et al. \[30\]](#), the  $Z$  parameter dependent ductility was reported for titanium alloys and aluminum alloy. For the tested material,  $Z$  parameter was also employed to represent the effect of temperature and strain rate on ductile fracture.  $Z$  parameter is formulated as:

$$Z = \dot{\epsilon} \exp\left(\frac{Q_{DRX}}{RT}\right) \quad (1)$$

where  $T$  is the temperature in the unit of Kelvins and  $\dot{\epsilon}$  is the strain rate.  $R$  is the gas constant which equals to  $8.314 \text{ J mol}^{-1} \text{ K}^{-1}$ .  $Q_{DRX}$  is the activation energy of DRX.

$Z$  parameter for the tested material was calibrated with results of hot compression tests. The determination of  $Z$  relies on the determination of  $Q_{DRX}$  and to calibrate  $Q_{DRX}$ , the Sellars creep function [\[33\]](#) was utilized to describe the relation between strain rate, stress, and temperature in hot deformation:

$$Z = \dot{\epsilon} \exp\left(\frac{Q_{DRX}}{RT}\right) = A \left[ \sinh(\alpha \sigma_p) \right]^n \quad (2)$$

where  $\sigma_p$  is the peak stress.  $A$ ,  $\alpha$  and  $n$  are material constants.  $\alpha$  can be calculated with the approximation of [Eq. \(2\)](#) and for the tested 316LN steel,  $\alpha$  equals to 0.01079.

Taking the logarithm of [Eq. \(2\)](#),  $Q_{DRX}$  is formulated as the following:

$$Q_{DRX} = R \left[ \frac{\partial \ln(\dot{\epsilon})}{\partial \ln(\sinh(\alpha \sigma_p))} \right]_{T=const} \left[ \frac{\partial \ln(\sinh(\alpha \sigma_p))}{\partial (T^{-1})} \right]_{\dot{\epsilon}=const} \quad (3)$$

The experimental data of hot compression tests and corresponding fitted curves of

$\partial \ln(\sinh(\alpha \sigma_p)) / \partial \ln(\dot{\epsilon})$  at constant temperature and  $\partial \ln(\sinh(\alpha \sigma_p)) / \partial (T^{-1})$  at constant strain rate are shown in Fig. 3. Slope of the fitted curves corresponds to the partial derivative in Eq. (3) and the average value of the slope was computed to determine  $Q_{DRX}$ .  $Q_{DRX}$  for the material was calculated as  $457665 \text{ J} \cdot \text{mol}^{-1}$ .

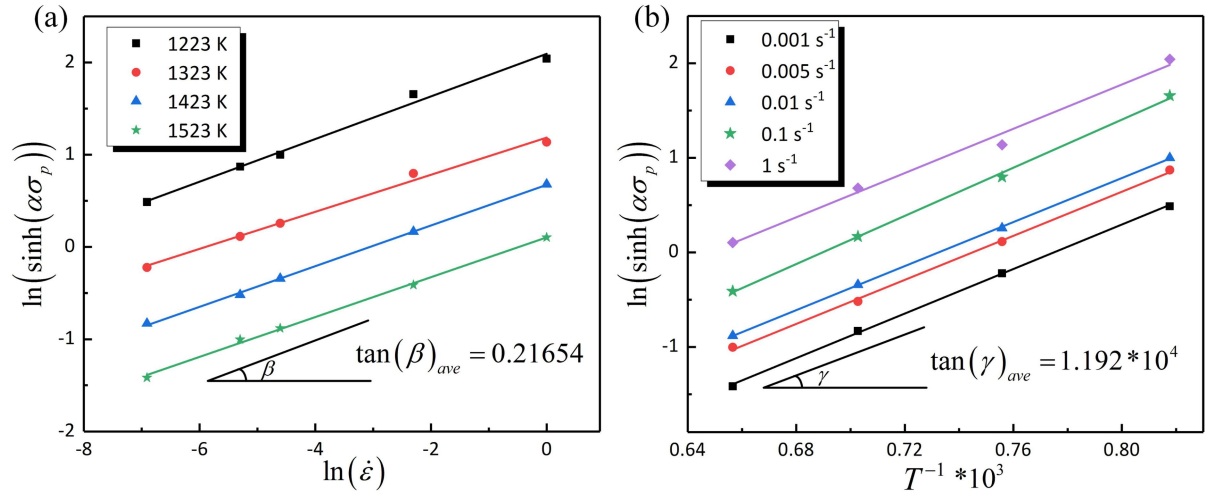


**Fig. 3.** Experimental data and corresponding fitted curves for results of hot compression tests:

(a)  $\ln(\sinh(\alpha \sigma_p)) - \ln(\dot{\epsilon})$ , and (b)  $\ln(\sinh(\alpha \sigma_p)) - T^{-1}$ .

## 2.4 Relationship between fracture strain and Z parameter in different DRX conditions

With the results of hot tensile experiments and hot compression tests, the relationship between fracture strain and Z parameter was obtained and shown in Fig. 4. For comparison, the fracture strain of dog-bone specimen in room temperature was also extracted and set as a reference. For hot tensile tests, when DRX does not occur in deformation, grains in the fracture region are elongated along the tensile direction and the fracture strain is close to the value at room temperature, such as in the test carried out at 1073 K - 1 s<sup>-1</sup>. However, when DRX happens in hot tensile process, fine and equiaxial grains form at the fracture zone, and the fracture strain becomes larger than that at room temperature. The fracture area in experiment conducted at 1373 K - 0.1 s<sup>-1</sup> is an example for DRX involved deformation. In

ductile materials, the formation of fracture is a process of void evolution. With the occurrence of DRX, void growth is greatly retarded due to the relief of local stress concentration caused by the energy-free DRX grains [32], and the ductility is thus improved by DRX. Via adopting  $Z$  parameter to represent the temperature and strain rate dependent DRX behavior, fracture strain presents a nearly monotonic decreasing trend with the increase of  $Z$  parameter.

In summary, the initiation condition of ductile fracture differs with DRX conditions. In deformation without DRX, the fracture strain is independent of  $Z$  parameter and approximates the value at room temperature. When DRX occurs, ductility of the material is improved and the relationship between fracture strain and the natural logarithm of  $Z$  parameter can be fitted by a linear function, as shown in Fig. 4. According to the above findings, the fracture strain in hot deformation of materials is described as:

$$\begin{cases} \bar{\varepsilon}_f = \bar{\varepsilon}_{rf} & \text{Without DRX} \\ \bar{\varepsilon}_f = \bar{\varepsilon}_{rf} [A - B * \ln(Z)] & \text{DRX region} \end{cases} \quad (4)$$

where  $\bar{\varepsilon}_{rf}$  is the fracture strain at room temperature.  $A$  and  $B$  are material constants.

For characterizing DRX initiation, the critical strain was used as the representative parameter:

$$\varepsilon_c = 0.0004Z^{0.1553} \quad (5)$$

As the fracture strain  $\bar{\varepsilon}_f$  in Eq. (4) is discontinuous in the transition point  $\varepsilon_c$ , the percentage of DRX,  $X_{drx}$ , was incorporated into the formulation of  $\bar{\varepsilon}_f$  as a weighting function for fracture strain in different DRX conditions:

$$\begin{cases} \bar{\varepsilon}_f = \bar{\varepsilon}_{rf} & \varepsilon < \varepsilon_c \\ \bar{\varepsilon}_f = \bar{\varepsilon}_{rf} [(1 - X_{drx}) + (A - B * \ln(Z)) X_{drx}] & \varepsilon \geq \varepsilon_c \end{cases} \quad (6)$$

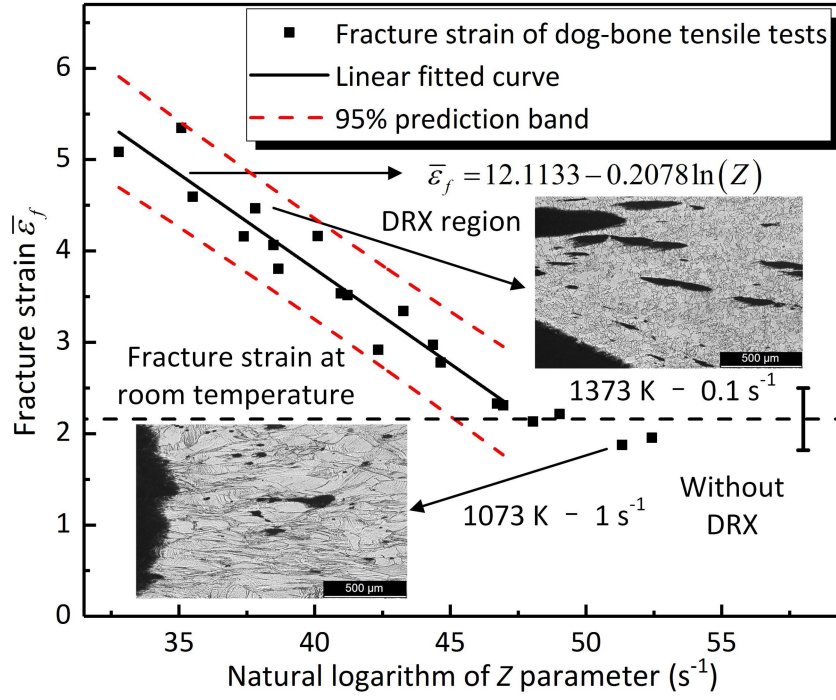


**Fig. 4.** Relationship between fracture strain and  $Z$  parameter in different DRX scenarios.

For the tested material,  $X_{drx}$  was formulated as [32]:

$$X_{drx} = 1 - \exp \left( -0.4437 \left( \frac{\varepsilon - \varepsilon_c}{\varepsilon_p} \right)^{1.192} \right) \quad (\varepsilon \geq \varepsilon_c) \quad (7)$$

### 3. Establishment of ductile fracture model for hot metal forming

#### 3.1 Extended ductile fracture model considering stress state and $Z$ parameter

In plastic deformation of metallic materials, the initiation of ductile fracture is also affected by stress state. Different stress states result in different fracture modes. In condition of high stress triaxiality, ductile fracture forms with the necking of material's internal void, while in low stress triaxiality scenario, it forms with the shear localization [34-37]. For modeling of ductile fracture, the stress triaxiality was considered in earlier research works, such as the classical Oyane model [3] and Ayada model [4]. The shear effect on ductile fracture began to be emphasized with the experimental findings that the ductility of materials was not in a

monotonic relation with stress triaxiality [6, 38-40]. To incorporate the shear effect, the Lode parameter was utilized as a representative parameter for shear deformation and taken into account in ductile fracture modeling [8-11]. In this study, the fracture criterion proposed by Lou et al. [10, 11] which contains both the influence of stress triaxiality and Lode parameter was adopted as the basis for model development. Efficiency of the model in capturing the onset of ductile fracture in a wide stress range has been demonstrated by experiments [38] and the fracture criterion is formulated as:

$$\bar{\varepsilon}_{lf} = \frac{C_3}{\left(\frac{2}{\sqrt{L^2+3}}\right)^{C_1} \left(\frac{\langle 1+3\eta \rangle}{2}\right)^{C_2}} \quad \langle x \rangle = \begin{cases} x & x \geq 0 \\ 0 & x < 0 \end{cases} \quad (8)$$

where  $C_1 \sim C_3$  are material constants.  $\eta$  is stress triaxiality and  $L$  is Lode parameter:

$$\eta = \frac{\sigma_m}{\bar{\sigma}} \quad (9)$$

$$L = \frac{2\sigma_2 - \sigma_1 - \sigma_3}{\sigma_1 - \sigma_3} \quad (10)$$

where  $\sigma_m$  and  $\bar{\sigma}$  are the mean stress and equivalent stress.  $\sigma_1$ ,  $\sigma_2$  and  $\sigma_3$  are principle stresses with the sequence of  $\sigma_1 \geq \sigma_2 \geq \sigma_3$ .  $L$  is related to the third invariant of deviatoric stress  $J_3$ :

$$\frac{(L(L-3)(L+3))^{1/3}}{\sqrt{L^2+3}} \bar{\sigma} = \left(\frac{27}{2} J_3\right)^{1/3} \quad (11)$$

The range of  $L$  is between  $-1$  and  $1$ .  $L=1$  or  $L=-1$  represents the axisymmetric stress state and  $L=0$  corresponds to the state of a pure shear plus a hydrostatic stress. In deformation with a constant  $\eta$ ,  $\bar{\varepsilon}_{lf}$  gets minimum at  $L=0$ , and peaks when  $|L|=1$ . As for the cut-off value of  $\eta$ ,  $\bar{\varepsilon}_{lf}$  becomes infinite when  $\eta$  is smaller than  $-1/3$ . Therefore,

ductile fracture will not occur in deformation with  $\eta \leq -1/3$ .

By introducing the relationship among fracture strain,  $Z$  and  $X_{drx}$  into Eq. (8),  $\bar{\varepsilon}_{Lf}$  is extended to hot deformation:

$$\left\{ \begin{array}{ll} \bar{\varepsilon}_{hLf} = \frac{C_3}{\left(\frac{2}{\sqrt{L^2+3}}\right)^{C_1} \left(\frac{\langle 1+3\eta \rangle}{2}\right)^{C_2}} & \varepsilon < \varepsilon_c \\ \bar{\varepsilon}_{hLf} = \frac{C_3}{\left(\frac{2}{\sqrt{L^2+3}}\right)^{C_1} \left(\frac{\langle 1+3\eta \rangle}{2}\right)^{C_2}} \left[ (1-X_{drx}) + (A-B*\ln(Z))X_{drx} \right] & \varepsilon \geq \varepsilon_c \end{array} \right. \quad (12)$$

For the deformation with non-proportional loading path or inconstant temperature and strain rate, the damage accumulation can be characterized by an integral form of strain increment:

$$D_{hL} = \int_0^{\bar{\varepsilon}_{hLf}} \frac{1}{\bar{\varepsilon}_{hLf}(\eta, L, Z, X_{drx})} d\bar{\varepsilon} \quad (13)$$

where  $D_{hL}$  is the damage factor. Ductile fracture takes place when  $D_{hL}$  reaches unity.

### 3.2 Calibration of stress state related parameters

For the established fracture model in Eqs. (12) and (13),  $C_1$ ,  $C_2$  are stress state related parameters and were calibrated via experiments with different stress conditions. In deformation at room temperature, ductility of the material is independent of strain rate and only affected by stress state. Therefore, the stress dependent material constants were determined by room temperature tests with different types of specimens. The cylinder notched samples with different notch radii (NR20, NR10, NR5) and plate samples with different widths and notched lengths (PT6, PT4) were applied, as shown in Fig. 5(a). Stress variables of the tests were identified via FE simulation and the stress-strain relation adopted

for simulation was determined with the result of dog-bone tension by using the trial-and-error approach [6]. Corresponding stress state of room temperature experiments and representative stress state of plane stress ( $\sigma_1=0$  or  $\sigma_2=0$ , or  $\sigma_3=0$ ), plane strain ( $\sigma_2=\sigma_m$ ), and axisymmetric stress ( $\sigma_1=\sigma_2$  or  $\sigma_2=\sigma_3$ ) are drawn in stress space of  $(\eta, L)$  in Fig. 5(b).

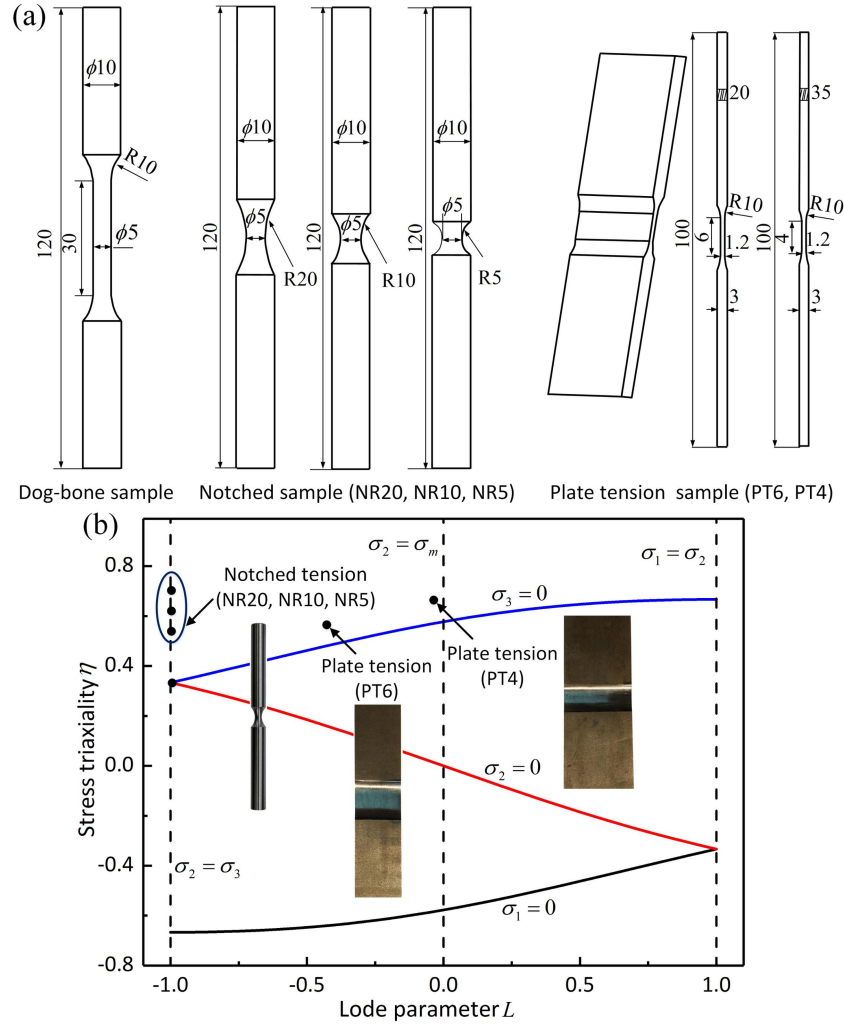


**Fig. 5.** Design of room temperature experiments: (a) Specimen shape and dimension, and (b) Stress state of the experiments in space of  $(\eta, L)$ .

The evolution of stress variables was examined for room temperature experiments, and the variation of stress condition results in the variation of ductile fracture behavior. Experiments of NR10 and PT4 were taken as representatives for notched and plate tension, and the

parameter evolution for critical element in the tests is shown in Fig. 6. For NR10 sample,  $L$  remains  $-1$  during deformation, indicating that the central area is in an axisymmetric tensile state and the high  $\eta$  is the dominated factor for void evolution and damage accumulation [36]. As for the PT4 specimen, the value of  $L$  approximates  $0$  and the stress state is close to plane strain. In this deformation scenario, the void shearing effect caused by deviatoric stress also contributes to the increase of damage [15]. As  $\eta$  and  $L$  vary with deformation, the average value of  $\eta$  and  $L$  was calculated for parameter calibration [38]:

$$\eta_{ave} = \frac{1}{\bar{\varepsilon}_f} \int_0^{\bar{\varepsilon}_f} \eta d\varepsilon \quad (14)$$

$$L_{ave} = \frac{1}{\bar{\varepsilon}_f} \int_0^{\bar{\varepsilon}_f} L d\varepsilon \quad (15)$$

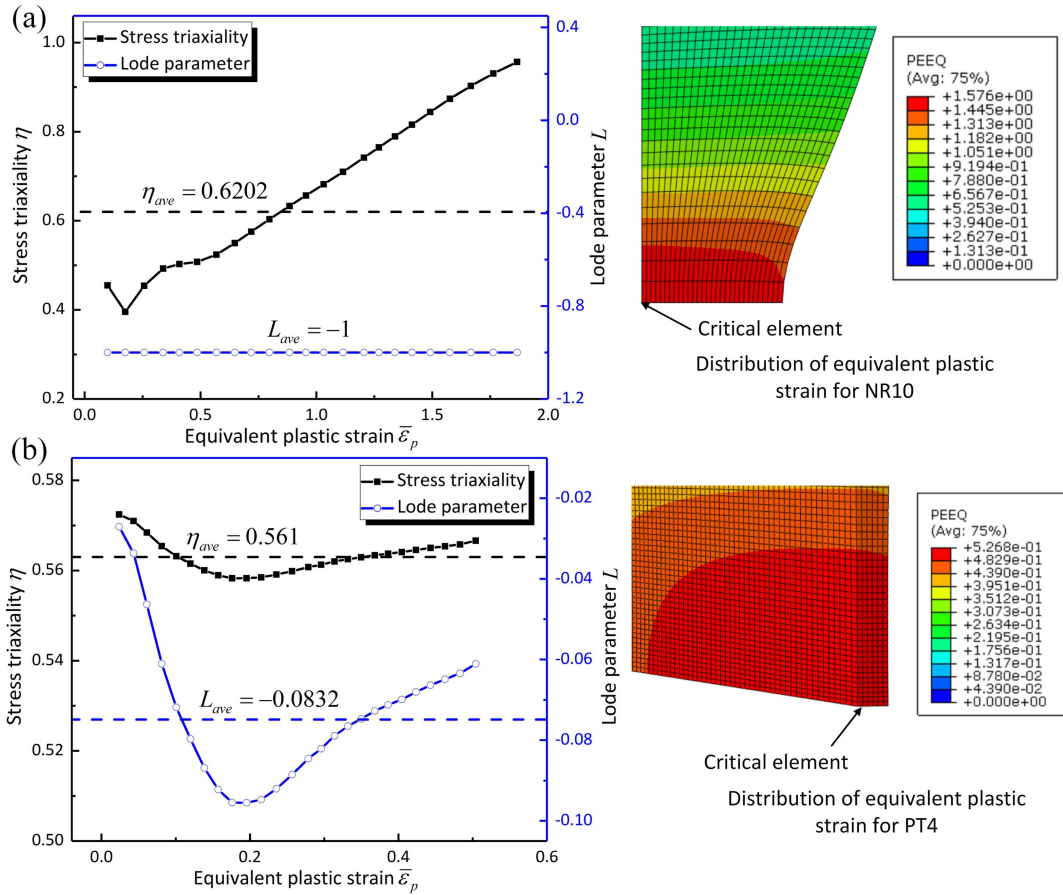


**Fig. 6.** Evolution of stress triaxiality and Lode parameter for room temperature experiments: (a) NR10, and (b) PT4.



Stress dependent parameters in the developed model was calibrated with the simulated results of  $\eta$ ,  $L$  and  $\bar{\varepsilon}_f$  listed in Table 3. According to the simulated consequences, the notched tests of NR20, NR10 and NR5 possess the same  $L$  but different values of  $\eta$ . Therefore, the notched experiments were adopted to calibrate  $\eta$  related parameter in the established model, i.e., parameter  $C_1$  in Eq. (12). Fig. 7(a) presents the data of notched tests and corresponding fitted curve of  $\bar{\varepsilon}_{hLf}$  for determining  $C_1$ . As for parameter  $C_2$  in the extended model, which represents the effect of  $L$  on ductile fracture, experiments of plate tension (PT4, PT6) and notched tension NR10 with different values of  $L$  were selected for calibration. As  $\eta$  also varies in the experiments, fracture strain of PT4 and PT6 was converted to the value at the same  $\eta$  as NR10 and the fitted curve for  $\bar{\varepsilon}_{hLf}$  at a constant  $\eta$  is shown in Fig. 7(b). With the calibration procedure discussed above, stress related parameters were determined for the tested material with  $C_1$  equivalent to 3.051 and  $C_2$  equivalent to 1.181.

**Table 3**

Stress triaxiality, Lode parameter and fracture strain for room temperature tests.

Specimen	Stress triaxiality	Lode parameter	Fracture strain
NR20	0.5826	-1	1.6245
NR10	0.6202	-1	1.5526
NR5	0.6796	-1	1.4424
PT6	0.4561	-0.5278	1.409
PT4	0.561	-0.0832	1.0953

Special attention should be paid to the inefficiency of FE simulation in capturing local strain concentration of experiments with a large uniform deformation zone. For instance, the simulated fracture strain of dog-bone test is smaller than the value calculated by the extended

fracture model shown in Fig. 7 even the mesh is refined in central area of the specimen. This variation is derived from the fact that in experiment with uniform deformation, fracture initiates at the area where small defects, such as voids and inclusions exist. However, the physical defects are not included in simulation and the simulated fracture strain for uniform deformation is thus smaller than the true value. To deal with the issue, a modification factor was multiplied on the simulated fracture strain of experiment with a large uniform deformation area, including the dog-bone test and the plate tension specimen.

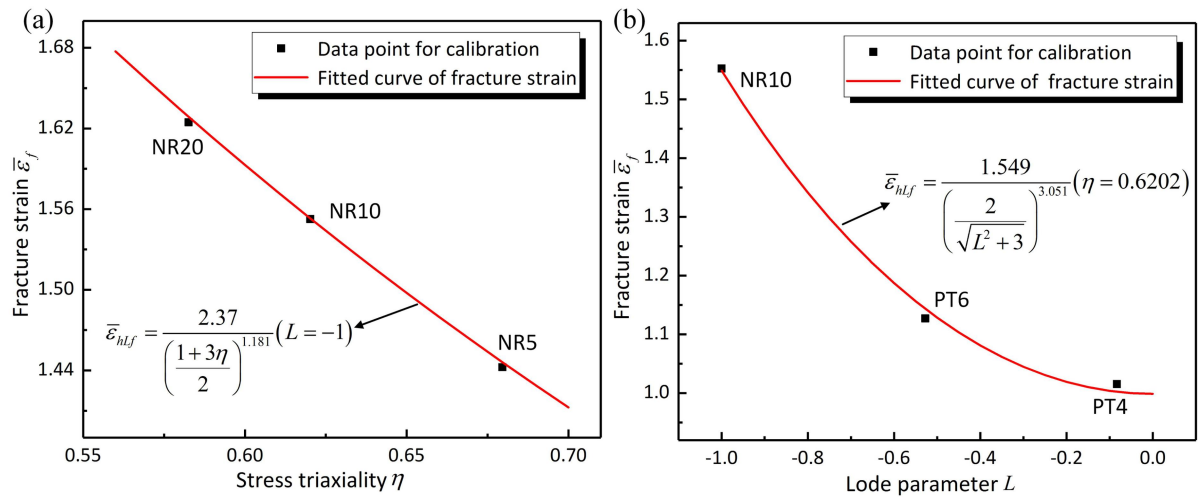


**Fig. 7.** Data point and corresponding fitted curves of fracture strain for room temperature tests: (a) Determination of stress triaxiality related parameter, and (b) Determination of Lode parameter related parameter.

With the determined material constants for the tested material, the occurrence of fracture in hot deformation is described as:

$$\begin{cases} \bar{\epsilon}_{hlf} = \frac{2.37}{\left(\frac{2}{\sqrt{L^2 + 3}}\right)^{3.051} \left(\frac{1+3\eta}{2}\right)^{1.181}} & \epsilon < \epsilon_c \\ \bar{\epsilon}_{hlf} = \frac{2.37}{\left(\frac{2}{\sqrt{L^2 + 3}}\right)^{3.051} \left(\frac{1+3\eta}{2}\right)^{1.181}} \left[ (1 - X_{drx}) + (5.2643 - 0.0903 * \ln(Z)) X_{drx} \right] & \epsilon \geq \epsilon_c \end{cases} \quad (16)$$

By introducing  $\bar{\varepsilon}_{hLf}$  into the expression of damage factor in Eq. (13), extended DFC for hot metal forming was established. The model was then embedded into ABAQUS/Explicit via user subroutine VUMAT to simulate hot working process and predict fracture initiation.

#### 4. Validation and application

To validate the reasonability and efficiency of the developed model, validation experiments with different types of specimens and hot working parameters were designed and conducted, as shown in Fig. 8. The hot notched specimen (HNR10) was used to construct high stress triaxiality and the hot plate tension (HPT10) was to produce a plain strain condition. The stress state for hot tension-shear specimens (HTS) is between uniaxial tension and pure shear, and the performance of the developed model in complex stress status can thus be analyzed with HTS samples. In addition, different temperatures and deformation rates induce different DRX conditions. To identify the fracture initiation situation and the influence of stress,  $Z$  parameter and DRX on ductile fracture, simulation was conducted for validation experiments.

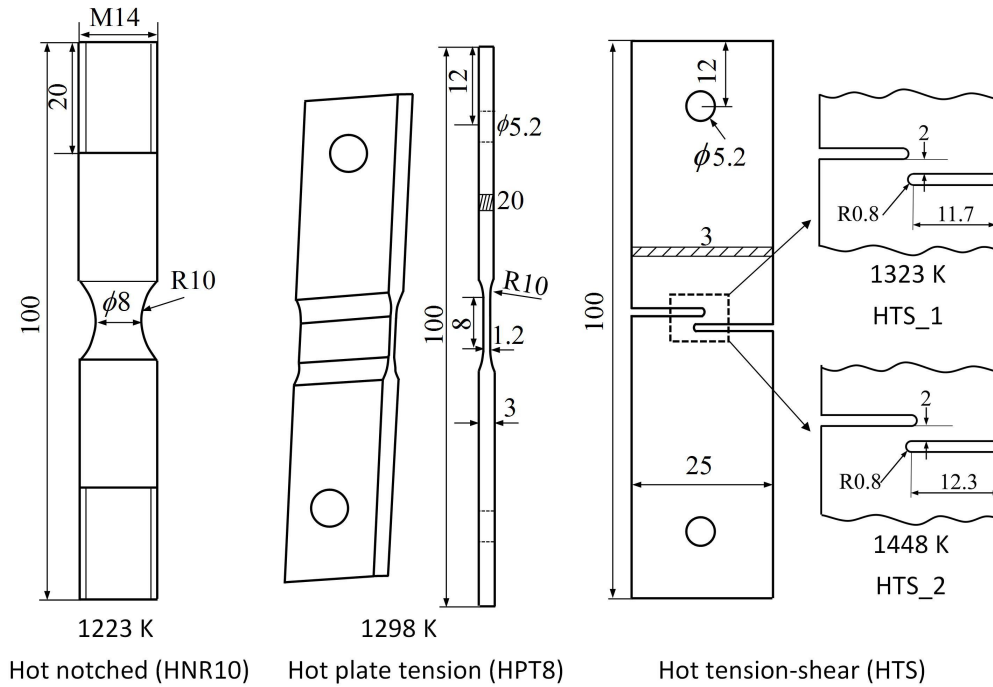


**Fig. 8.** Specimens and test conditions for validation experiments.

The parameter evolution and comparison of load-stroke curves for validation experiments of HNR10 and HPT8 were examined and presented in Fig. 9. According to the simulation results, the maximum damage factor appears at center of the necking zone, which is called the critical element hereby. In deformation of the tests,  $D_{hL}$  undergoes a smooth increase and  $\bar{\varepsilon}_{hLf}$  varies with deformation, as shown in Fig. 9(a). The change of  $\bar{\varepsilon}_{hLf}$  is related to the change of stress states,  $Z$  and  $X_{drx}$  exhibited in Fig. 9(b) and (c). For the HNR10 test, where  $L$  maintains zero and  $\ln(Z)$  increases slightly in deformation, the change of  $\bar{\varepsilon}_{hLf}$  is from the comprehensive effect of  $\eta$  and  $X_{drx}$ . As for the test of HPT8, the stress state is relatively stable and the main influential factors of  $\bar{\varepsilon}_{hLf}$  are  $Z$  and  $X_{drx}$ . As  $\bar{\varepsilon}_{hLf}$  is independent of  $Z$  and  $X_{drx}$  in deformation without DRX,  $\bar{\varepsilon}_{hLf}$  remains almost constant in pre-DRX stage of the HPT8 experiment. When DRX occurs,  $\bar{\varepsilon}_{hLf}$  becomes larger due to the rapid growth of  $X_{drx}$ .  $\bar{\varepsilon}_{hLf}$  decreases in final stage of deformation when  $X_{drx}$  becomes stable and  $\ln(Z)$  undergoes an obvious increase. As indicated in Fig. 9(d), the simulated load-stroke agrees well with experimental results and the predicted fracture point for both the HNR10 and HPT8 test lies on the significant drop of the load-stroke curve. Therefore, the extended fracture model is efficient in capturing the onset of ductile fracture in different working conditions.

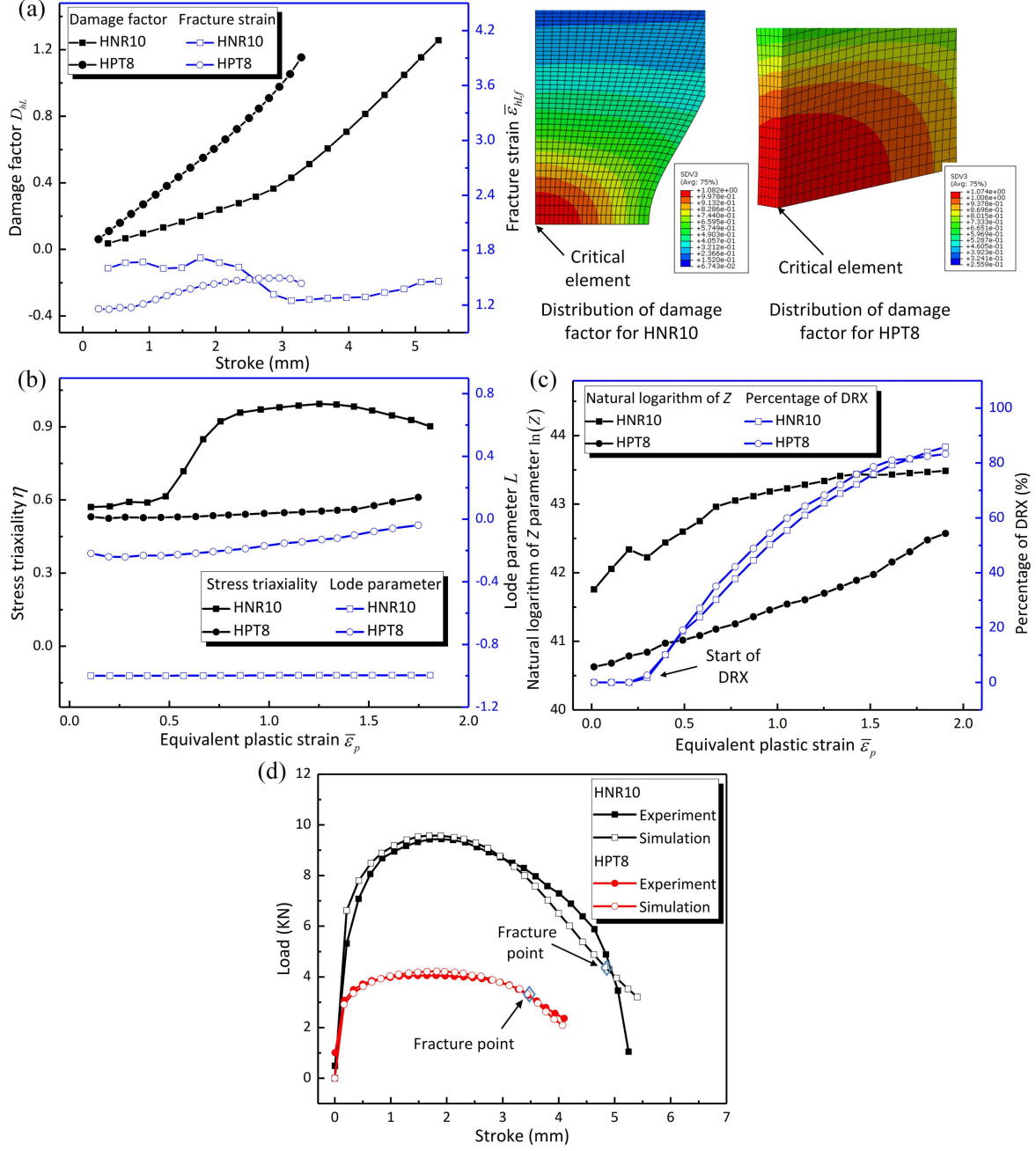


**Fig. 9.** Parameter evolution and load-stroke comparison for HNR10 and HPT8: (a) Damage factor and fracture strain, (b) Stress triaxiality and Lode parameter, (c) Natural logarithm of Z parameter and the percentage of DRX, and (d) Comparison of load-stroke curves between experimental and simulated results.

Performance of the developed model was further identified via HTS experiments. In the simulated results of HTS tests, deformation concentrates in ligament of HTS specimens and

fracture initiates from middle surface along thickness of the samples. With predictions of the extended model shown in Fig. 10(a), an almost simultaneous fracture takes place at central as well as edge area of the HTS\_1 sample while only the edge of the HTS\_2 sample is predicted as the critical region for fracture occurrence. The influential factors for damage accumulation were examined for central and edge element and are presented in Fig. 10(b) to (e). In pre-DRX stage of the HTS\_1 test,  $\eta$  of the edge element is larger than that of the central element and the absolute value of  $L$  at the edge is more close to zero. Therefore, a faster increase of  $D_{hL}$  is shown at the edge. When DRX takes place with deformation, the larger  $Z$  at the edge induces a faster growth of  $D_{hL}$  while the larger  $X_{drx}$  results in a slower growth of  $D_{hL}$ . In final deformation stage, due to the rapid growth of  $\eta$  at the central area,  $D_{hL}$  for central element undergoes a fast increase and ductile fracture occurs in central as well as edge area of the HTS\_1 sample almost at the same time. As for the HTS\_2 test, DRX happens in early stage of deformation and  $X_{drx}$  at edge of the ligament is larger than that at the center area. Nevertheless, with the larger  $\eta$  and  $Z$ , and smaller absolute value of  $L$  for edge element during most of the tensile deformation,  $D_{hL}$  remains higher at the edge until the fracture point.

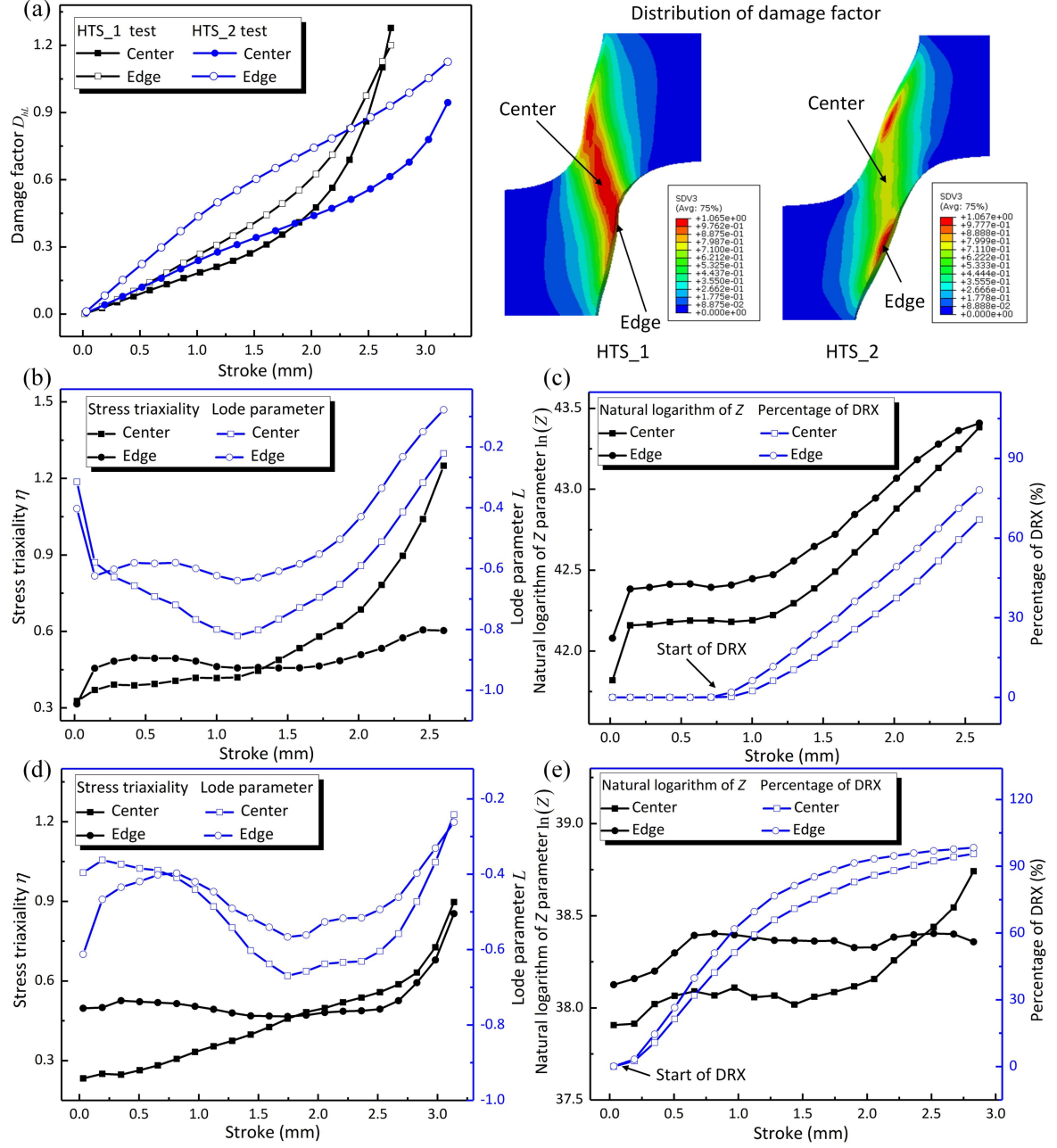


**Fig. 10.** Parameter evolution for HTS experiments: (a) Damage factor, (b) Stress triaxiality and Lode parameter for HTS\_1 test, (c) Natural logarithm of Z parameter and percentage of DRX for HTS\_1 test, (d) Stress triaxiality and Lode parameter for HTS\_2 test, and (e) Natural logarithm of Z parameter and percentage of DRX for HTS\_2 test.

Propagation of ductile fracture predicted by the developed model was also analyzed for HTS tests, as shown in Fig. 11. For the HTS\_1 experiment, ductile fracture takes place at center as

well as edge of the specimen and propagates through the ligament, forming a slant fracture with respect to the tensile direction. With regard to the test of HTS\_2, the edge area is predicted as the fracture initiation zone. However, as edge fracture is not easy to propagate, fracture also occurs in interior of the ligament during subsequent deformation and the complete failure forms with the combination of central and edge fracture in HTS\_2 sample. The extended model can thus capture the initiation as well as the propagation of fracture in hot working of metallic materials.

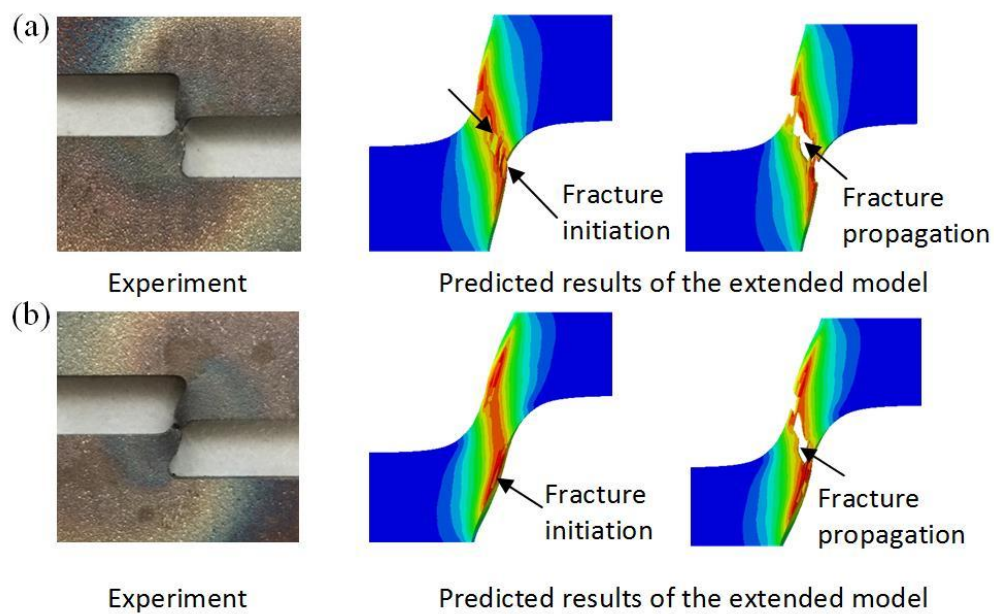


**Fig. 11.** The experimental and simulated fracture zone of HTS tests: (a) The HTS\_1 sample, and (b) The HTS\_2 sample.

As an instance for industrial application, the developed fracture model was applied to the hot forging process of a pressure vessel cap. Pressure vessel is key component in nuclear power equipment which is of high quality requirement. In practical production, the multi-pass hot forging technology was utilized to make qualified head cover of pressure vessels and this forming process was simulated in ABAQUS by using thermal-mechanical coupled approach. To form the head cover, tailor designed workpiece was deformed by repeated movements and rotations of top die and the initial assembly of workpiece and dies is shown in Fig. 12(a).



Mesh of the workpiece was refined to acquire an accurate result and the refined mesh is presented in Fig. 12(b). As indicated in Fig. 13(a), the central area at bottom of the workpiece is predicted as the critical region for fracture occurrence and the evolution of damage factor for critical element is shown in Fig.13(b). Damage accumulates in forming stage of the head cover when top die is in contact of the workpiece and the value of  $\eta$  for critical area is larger than  $-1/3$ . After six passes of forging, the damage factor still lies in a safe range and this forming technology is thus crack-free. However, care must be taken to the possibility of fracture occurrence if further deformation is conducted. Besides, in the situation of forming technology adjustment, the working process should be re-simulated.

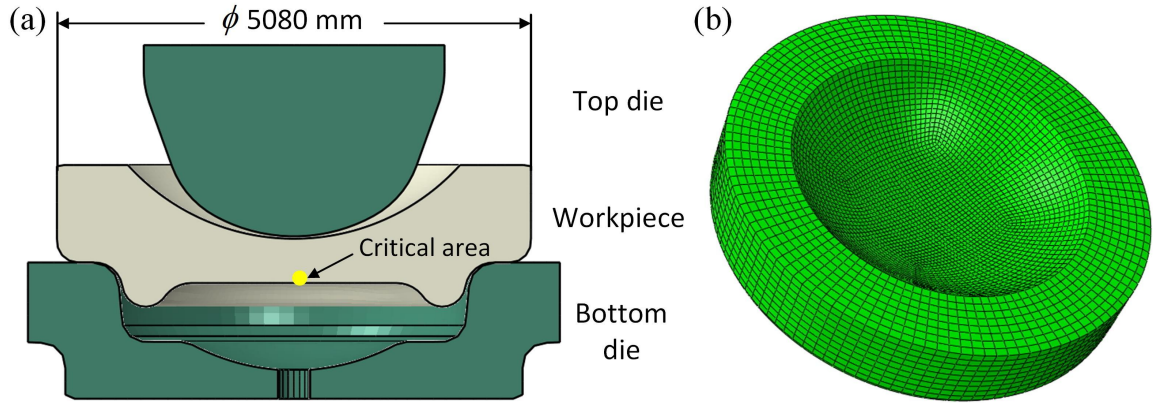


**Fig. 12.** FE model for hot forging of the pressure vessel cap: (a) Half of the initial assembly, and (b) Refined mesh of the workpiece.

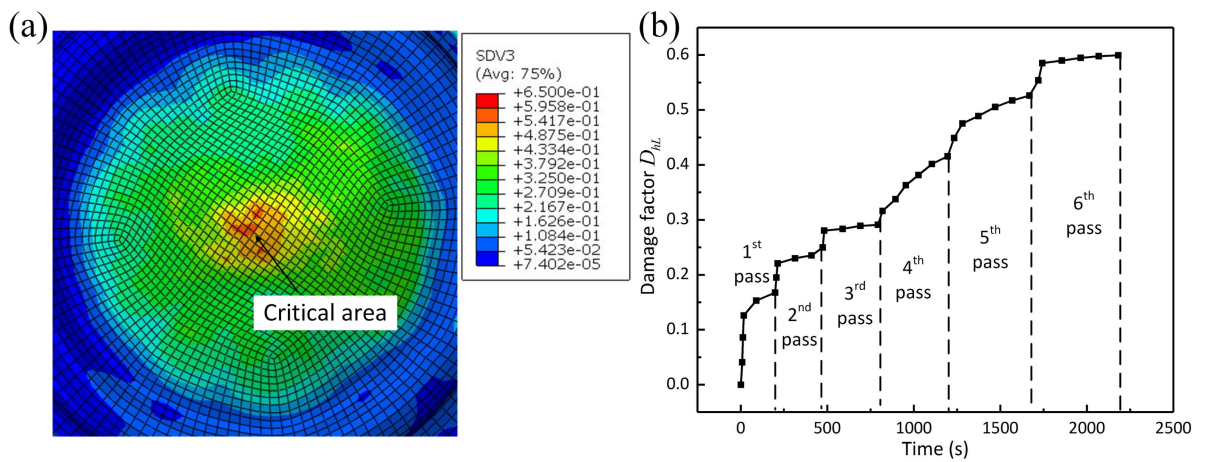


**Fig. 13.** Damage factor in the multi-pass hot forging: (a) Distribution of the damage factor after the sixth forging pass, and (b) Evolution of damage factor for critical element.

## 5. Conclusions

In this study, a comprehensive investigation on ductile fracture in hot deformation of 316LN steel was provided and an extended model for predicting fracture occurrence in deformation of metallic materials at elevated temperatures was established. The following conclusions can be drawn accordingly:

(1) Accompanied with the grain refinement in DRX, the ductility of metallic materials is improved by DRX. By using  $Z$  parameter to characterize the combined effect of temperature and strain rate on DRX, it is demonstrated that the fracture strain is decreased with the increase of  $Z$  parameter in deformation with DRX. Nevertheless, when DRX does not occur in the deformation, the fracture strain presents an independency on  $Z$  parameter.

(2) Through incorporating  $Z$  parameter and the influence of DRX into a stress based fracture model, an extended ductile fracture model for hot forming of metallic materials was established. In the developed model, the fracture strain in the DRX involved deformation is dependent on stress state,  $Z$  parameter and the percentage of DRX. A linear relation was used to describe the relationship between fracture strain, the natural logarithm of  $Z$  parameter, and the percentage of DRX was introduced as a weighting function. As for deformation without DRX, the fracture strain was expressed as a function of stress triaxiality and Lode parameter. The extended model considers the influences of stress triaxiality, Lode parameter,  $Z$  parameter as well as DRX, and is able to predict fracture occurrence in hot working of materials with a wide parameter range of stress state, temperature and strain rate. By implementing the model into FE code, the ductile fracture behavior in hot deformation can thus be analyzed.

(3) Furthermore, the validation experiments were designed and conducted, and the results demonstrated that the established model is efficient in capturing the onset and the propagation of fracture in tensile as well as shear dominated hot deformation. As a case study

of industrial application, the developed model was applied to a multi-pass hot forging of a pressure vessel cap to identify the critical region and the possibility of thermal fracture initiation. The model was thus validated and verified to be a promising DFC in hot working of metallic materials.

### **Acknowledgements**

The authors gratefully acknowledge the financial support from the National Natural Science Foundation of China with the projects of Nos. 51675335 and 51575465. This work is also carried out with the support from the project of B-Q55M (152792/16E) from the RGC of Hong Kong Government.

### **References**

- [1] Khan A S, Liu H. Strain rate and temperature dependent fracture criteria for isotropic and anisotropic metals. *Int. J. Plast.* 2012;37:1-15.
- [2] Cockcroft M G, Latham D J. Ductility and the workability of metals. *J Inst Metals* 1968;96:33-39.
- [3] Oyane M. Criteria of DF strain. *Bull. JSME* 1972;15:1507-1513.
- [4] Ayada M, Higashino T, Mori K. Central bursting in extrusion of inhomogeneous materials, ICTP 1987-Proceedings of the 2nd International Conference on Technology of Plasticity, Stuttgart, Germany, 1987, pp. 553-558.
- [5] Brozzo P, DeLuca B, Rendina R. A new method for the prediction of formability in metal sheets. In: *Proceedings of the 7th Biennial Conference of the International Deep Drawing Research Group on Sheet Metal Forming and Formability* 1972.
- [6] Bao Y. Prediction of ductile crack formation in uncracked bodies. America: Massachusetts Institute of Technology; 2003 (Ph.D. thesis).
- [7] Bai Y. Effect of loading history on necking and fracture. America: Massachusetts Institute of Technology; 2008 (Ph.D. thesis).

- [8] Xue L. Damage accumulation and fracture initiation in uncracked ductile solids subject to triaxial loading. *Int. J. Solids Struct.* 2007;44:5163-5181.
- [9] Bai Y, Wierzbicki T. A new model of metal plasticity and fracture with pressure and Lode dependence. *Int. J. Plast.* 2008;24:1071-1096.
- [10] Lou Y, Huh H, Lim S, Pack K. New ductile fracture criterion for prediction of fracture forming limit diagrams of sheet metals. *Int. J. Solids Struct.* 2012;49:3605-3615.
- [11] Lou Y, Huh H. Extension of a shear-controlled ductile fracture model considering the stress triaxiality and the Lode parameter. *Int. J. Solids Struct.* 2013;50:447-455.
- [12] Tvergaard V, Needleman A. Analysis of the cup-cone fracture in a round tensile bar. *Acta Metall.* 1984;32:157-169.
- [13] Tvergaard V. Influence of voids on shear band instabilities under plane strain conditions. *Int. J. Fract.* 1981;17:389-407.
- [14] Gurson A L. Continuum theory of ductile rupture by void nucleation and growth: Part I—Yield criteria and flow rules for porous ductile media. *J. Eng. Mater. Technol.* 1977;99:2-15.
- [15] Xue L. Constitutive modeling of void shearing effect in ductile fracture of porous materials. *Eng. Frac. Mech.* 2008;75:3343-3366.
- [16] Nahshon K, Hutchinson J W. Modification of the Gurson Model for shear failure. *Eur. J. Mech. A* 2008;27:1-17.
- [17] Xu Z T, Peng L F, Fu M W, Lai X M. Size effect affected formability of sheet metals in micro/meso scale plastic deformation: Experiment and modeling. *Int. J. Plast.* 2015;68:34-54.
- [18] Malcher L, Andrade Pires F M, César de Sá J M A. An extended GTN model for ductile fracture under high and low stress triaxiality. *Int. J. Plast.* 2014;54:193-228.
- [19] Li H, Fu M W, Lu J, Yang H. Ductile fracture: Experiments and computations. *Int. J. Plast.* 2011;27:147-180.

- [20] Wierzbicki T, Bao Y, Lee Y-W, Bai Y. Calibration and evaluation of seven fracture models. *Int. J. Mech. Sci.* 2005;47:719-743.
- [21] Ma H, Xu W, Jin B C, Shan D, Nutt S R. Damage evaluation in tube spinnability test with ductile fracture criteria. *Int. J. Mech. Sci.* 2015;100:99-111.
- [22] Msolli S, Badreddine H, Labergere C, Martiny M, Robin G, Jrad M, Saanouni K, Choquart F. Experimental characterization and numerical prediction of ductile damage in forming of AA1050-O sheets. *Int. J. Mech. Sci.* 2015;99:262-273.
- [23] Said L B, Mars J, Wali M, Dammak F. Numerical prediction of the ductile damage in single point incremental forming process. *Int. J. Mech. Sci.* 2017;131-132:546-558.
- [24] Johnson G R, Cook W H. Fracture characteristics of three metals subjected to various strains, strain rates, temperatures and pressures. *Eng. Frac. Mech.* 1985;21:31-48.
- [25] Valoppi B, Bruschi S, Ghiotti A, Shivpuri R. Johnson-Cook based criterion incorporating stress triaxiality and deviatoric effect for predicting elevated temperature ductility of titanium alloy sheets. *International Journal of Mechanical Sciences* 2017;123:94-105.
- [26] He J, Cui Z, Chen F, Xiao Y, Ruan L. The new ductile fracture criterion for 30Cr2Ni4MoV ultra-super-critical rotor steel at elevated temperatures. *Mater. Des.* 2013;52:547-555.
- [27] Novella M F, Ghiotti A, Bruschi S, Bariani P F. Ductile damage modeling at elevated temperature applied to the cross wedge rolling of AA6082-T6 bars. *J. Mater. Process. Technol.* 2015;222:259-267.
- [28] Zhu Y, Zeng W, Zhang F, Zhao Y, Zhang X, Wang K. A new methodology for prediction of fracture initiation in hot compression of Ti40 titanium alloy. *Mater. Sci. Eng. A* 2012;553:112-118.
- [29] Oh S I, Chen C C, Kobayashi S. Ductile fracture in axisymmetric extrusion and drawing: Part 2, workability in extrusion and drawing. *Trans. ASME, J. Eng. Ind.* 1979;101:36-44.

- [30] Alexandrov S, Wang P T, Roadman R E. A fracture criterion of aluminum alloys in hot metal forming. *J. Mater. Process. Technol.* 2005;160:257-265.
- [31] Sun C Y, Guo N, Fu M W, Liu C. Experimental investigation and modeling of ductile fracture behavior of TRIP780 steel in hot working conditions. *Int. J. Mech. Sci.* 2016;110:108-115.
- [32] Shang X, Cui Z, Fu M W. Dynamic recrystallization based ductile fracture modeling in hot working of metallic materials. *Int. J. Plast.* 2017;95:105-122.
- [33] Sellars C M, Whiteman J A. Recrystallization and grain growth in hot rolling. *Met. Sci.* 1979;13:187-194.
- [34] Besson J. Continuum Models of Ductile Fracture: A Review. *International Journal of Damage Mechanics* 2009;19:3-52.
- [35] Cao T S. Models for ductile damage and fracture prediction in cold bulk metal forming processes: a review. *International Journal of Material Forming* 2017;10:139-171.
- [36] Ueda T, Helfen L, Morgeneyer T F. In situ laminography study of three-dimensional individual void shape evolution at crack initiation and comparison with Gurson–Tvergaard–Needleman-type simulations. *Acta Mater.* 2014;78:254-270.
- [37] Weck A, Wilkinson D S. Experimental investigation of void coalescence in metallic sheets containing laser drilled holes. *Acta Mater.* 2008;56:1774-1784.
- [38] Lou Y. A new ductile fracture criterion for the formability prediction of steel sheets and its application to finite element analysis. Korea: Korea Advanced Institute of Science and Technology; 2012 (Ph.D. thesis).
- [39] Dunand M, Mohr D. On the predictive capabilities of the shear modified Gurson and the modified Mohr–Coulomb fracture models over a wide range of stress triaxialities and Lode angles. *J. Mech. Phys. Solids* 2011;59:1374-1394.
- [40] Gao X, Zhang T, Hayden M, Roe C. Effects of the stress state on plasticity and ductile

failure of an aluminum 5083 alloy. *Int. J. Plast.* 2009;25:2366-2382.